Structural and Spectroelectrochemical Study of Carbonate and Bicarbonate Adsorbed on Pt(111) and Pd/Pt(111) Electrodes

Antonio Berná, Antonio Rodes,* and Juan M. Feliu

Departamento de Química Física e Instituto Universitario de Electroquímica, Universidad de Alicante, Apartado 99, 03080 Alicante, Spain

Francesc Illas

Departament de Química Física i Centre de Recerca en Química Teòrica, Universitat de Barcelona i Parc Científic de Barcelona, C/Martí i Franquès 1, 08028 Barcelona, Spain

Alfred Gil, Anna Clotet, and Josep M. Ricart*

Departament de Química Física i Inorgànica, Universitat Rovira i Virgili, Pl. Imperial Tàrraco 1, 43005 Tarragona, Spain

Received: May 4, 2004; In Final Form: September 6, 2004

Spectroelectrochemical experiments and density functional theory (DFT) based calculations are combined to elucidate the nature of the species adsorbed when a perchloric acid solution saturated with carbon dioxide is in contact with well-defined electrode surfaces. Previous results reported for the Pt(111) electrode are revised and completed with new data for a palladium monolayer deposited on the Pt(111) electrode. From the DFT calculations and from the potential and pH dependent behavior of the main adsorbate vibrational bands, it is suggested that, for potentials below 0.65 V, bicarbonate species are adsorbed at the Pt(111) electrode surface in a short-bridge bidentate configuration. At higher potentials, the adsorbate adlayer is completed by the formation of adsorbed carbonate also in a short-bridge configuration. The ratio between the surface coverages of adsorbed bicarbonate and carbonate depends on both the electrode potential and the solution pH. Adsorbed bicarbonate prevails at the palladium monolayer irrespective of the electrode potential. This behavior, together with a concomitant lower adsorbate coverage, can be related to the competitive adsorption of hydroxylated species.

1. Introduction

The specific adsorption of anions on surfaces in electrochemical environment has gained increasing attention in recent years because of its important role in the understanding of electrochemistry at a molecular level.[1−3] However, this is not a simple task because of the structural complexity of the electrode double layer. The application of surface science techniques in electrochemistry has triggered an important development in the detailed study of this kind of system.[2,3] In this context, the use of well-established procedures for the preparation of well-defined single-crystal electrode surfaces[4,5] has greatly simplified the study of structural aspects of electrochemical processes. At the same time, this type of study has taken advantage of the application of spectroscopic techniques to the investigation of the structure of adsorbed species at the electrode surface.[3] In particular, in situ Fourier transform infrared spectroscopy (FTIR) can be used in an electrochemical environment in a rather straightforward way.[6−8] Therefore, the interpretation of the infrared spectra obtained in electrochemical environment for several adsorbed anions has deserved considerable attention.[6,9−18] Among the studied anions, the infrared spectra for carbonate on Pt(110),[11,13] Pt(111),[12,13] and Au(111)[16] have been reported and discussed in the literature. Most often, the interpretation of these IR spectra is based on the comparison with the corresponding spectra of molecular complexes.[19] In carbonate, Markovits et al.[20] have shown that this comparison is not always straightforward and can lead to erroneous assignments. These authors have also shown that the vibrational frequency of the highest normal internal mode of A_1 symmetry can be assigned by comparison to the spectrum of carbonato molecular complexes whereas this comparison is not possible for other normal modes because of the presence of the surface. Hence, some normal modes are transferable from the complex to the surface adsorbed molecule whereas others are not.

The use of platinum single-crystal electrodes is well established and almost done in a routinely way. However, other metals present some difficulties when applied in an electrochemical environment. In Pd electrodes, this is mainly because electrochemical hydrogen absorption reaction confines the potential region where other electrochemical processes can be studied to quite a narrow range. However, it has been found that the deposition of a monolayer of palladium over other metallic electrodes, such as platinum or gold, can solve this problem, reducing the hydrogen absorption reaction in a great extent.[21] In this way, palladium-covered metallic electrodes supply a promising alternative to the use of bulk palladium single-crystal electrodes. In addition, palladium films deposited on well-ordered platinum or gold substrates may present interesting electrochemical properties. The preparation and

* Corresponding authors. E-mail: Antonio.Rodes@ua.es; Ricart@quimica.urv.es.

10.1021/jp048082r CCC: $27.50
Published on Web 10/22/2004

characterization of palladium films with different coverages ranging from submonolayers to multilayers have been extensively reported in the literature.[21−33] In addition, CO,[23,31,33] NO,[27] and (bi)sulfate[29,30] adlayers have been studied spectroscopically at palladium-modified Pt(111) electrodes. However, the number of experimental studies carried out using these Pd film electrodes is still scarce when compared to platinum or gold electrodes. In the present work, new experimental FTIR and electrochemical experiments are reported for (bi)carbonate species formed from CO_2-saturated solutions at Pt(111) electrodes and palladium monolayers deposited on Pt(111) (in the following, Pd/Pt(111) electrodes). These experiments, which include the study of the effect of solution pH on the infrared spectra of adsorbed species, have not been extended to Pt(100) and Pt(110) substrates since carbon dioxide is reduced at (110) and (100) sites to adsorbed carbon monoxide.[11,12,34] This experimental part is complemented by DFT model calculations which are used to help to understand the experimental data. The combined use of the two approaches permits to gain a detailed picture of the possible adsorbed species (i.e., carbonate or bicarbonate), adsorption site, and adsorption modes and also to assign the main features of the experimental spectra. In addition, a thorough comparison of the adsorption of (bi)carbonate species on bare and palladium-covered Pt(111) single-crystal electrodes is presented. Previous studies suggest that the interaction of carbonate with the Pt(111) surface involves a bidentate interaction[20] through a strong covalent bond. However, there is no information concerning the interaction of these species with Pd(111) and Pd/Pt(111) electrode surfaces.

2. Experimental Section

2a. Sample Preparation. Pt(111) single-crystal electrodes were prepared following the procedure described by Clavilier.[5] Samples employed for electrochemical experiments were about 2 mm in diameter whereas the diameter of the Pt(111) electrodes used for the in-situ infrared spectroscopy experiments were somewhat larger, ∼4.5 mm. Prior to any experiment, the working electrode was annealed in a gas-oxygen flame, cooled in a reductive atmosphere (H_2+Ar), and then transferred to the (spectro)electrochemical cell under the protection of a droplet of water saturated with these gases.[35] Experiments were carried out at room temperature.

Sulfuric and perchloric acid solutions were prepared from the concentrated acid (Merck Suprapur) and ultrapure water (Elga-Vivendi). In some of the spectroelectrochemical experiments, the working solutions were prepared in deuterium oxide (Merck, 99.95%) which was used as received. Potentials were measured against a reversible hydrogen electrode in the working solution (RHE). Prior to each experiment, the test solution was deareated by bubbling Ar (N50, L'Air Liquide). The electrochemical deposition of palladium was performed in a cell containing a 10^{-5} M Pd^{2+} solution in 0.l M H_2SO_4. Once a palladium coverage close to the monolayer was attained, the electrode was rinsed with ultrapure water and transferred to another cell containing a 0.1 M $HClO_4$ solution.[29−32] Cyclic voltammograms and charge displacement experiments were performed in this solution for the palladium-free and the palladium-covered Pt(111) electrode both in the absence and in the presence of carbon dioxide (N48, L'Air Liquide). The setup for the CO (N47, L'Air Liquide) charge displacement experiments has been described elsewhere.[36,37]

FTIR experiments were carried out with Nicolet Magna 850 spectrometer equipped with a narrow-band MCT detector. The spectroelectrochemical cell[38,8] was provided with a CaF_2 prismatic window bevelled at 60°. Spectra were collected at different electrode potentials either with p- or s-polarized light and a resolution of 8 cm^{-1}. The spectra are represented as the ratio $-\log(R/R_o)$ where R and R_o are the reflectance at the sample and reference potentials, respectively. The reference spectrum was collected at a potential between 0.10 and 0.30 V for which the electrode surface is free of (bi)carbonate anions (see below). Typically, 500 interferograms were coadded at each potential with the electrode potential being alternated from the reference to the sample potential every 100 interferograms. In some experiments, a higher number of interferograms was coadded to increase the signal-to-noise ratio in the resulting spectra.

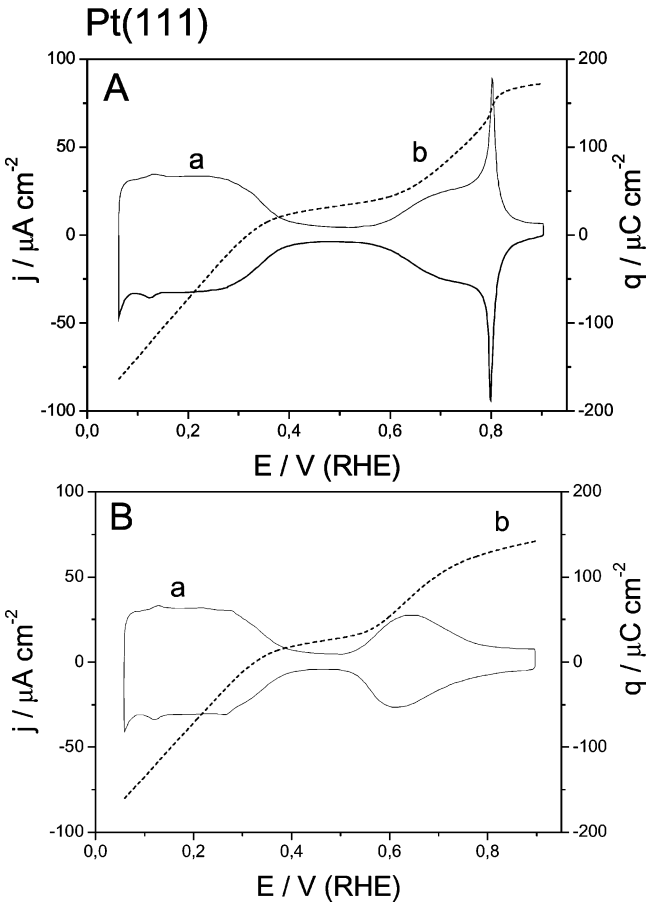

Figure 1. Cyclic voltammograms (a) and charge density curves (b) obtained for a Pt(111) electrode in (A) a CO_2-free and (B) a CO_2-saturated 0.1 M $HClO_4$ solution. Cyclic voltammograms were recorded at 0.05 V s^{-1} (same sweep rate in all figures).

2b. Experimental Results for Pt(111) Electrodes. Curve a in Figure 1A shows the typical cyclic voltammogram obtained for a well-ordered Pt(111) electrode in perchloric acid solution. Curve a in Figure 1B corresponds to the voltammetric curve obtained for the same electrode surface once the solution was saturated with carbon dioxide.

As previously discussed,[12,13] the main effects of the presence of carbon dioxide are the disappearance of the sharp voltammetric peaks at 0.78 V and the negative shift of the broad adsorption states, initially between 0.60 and 0.85 V. This voltammetric behavior is characteristic of the presence of adsorbed anions that replace the hydroxyl anions which are responsible for the voltammetric features observed for the Pt(111) electrode in contact with the CO_2-free perchloric acid solution. The relation between the adsorption states centered at ca. 0.65 V and the adsorption/desorption of anionic species can

also be derived from the charge density curves obtained by combining the voltammetric curves and charge displacement experiments in the presence of carbon dioxide. In the charge displacement experiments, gaseous CO is dosed on the electrode surface at a constant electrode potential giving rise to the quantitative displacement by adsorbed CO of any previously adsorbed species.[36,37] Taking into account that CO adsorption itself does not involve significant charge transfer,[36] the desorption of these species involves the transfer of the same charge density as in the adsorption process but with the opposite sign. The displaced charge, that flows through the external circuit and can be easily measured, can be taken as the total charge on the electrode surface at the dosing potential. Once the displaced charge density at a dosing potential E_1, $q_{dis}(E_1)$, is known, it may be used as an integration constant for the calculation of the total charge density at any other potential value, $q(E)$, through the integration of the voltammetric current density, $j(E)$, as follows:[39]

$$q(E) = \int_{E_1}^{E} \frac{|j(E)|}{\upsilon} dE - q_{dis}(E_1)$$

In this equation, υ stands for the scan rate. It can be accepted that $q_{dis}(E_1)$ is the opposite of the total charge at the potential E_1, $q(E_1)$.[40]

Curves b in Figure 1A and 1B correspond to the charge density curves obtained in the absence and in the presence of carbon dioxide, respectively. These curves reflect the changes in the nature and surface coverage of adsorbed species as a function of the electrode potential. Negative charges can be associated to the reductive adsorption of hydrogen

$$Pt(111) + H^+ + e \rightarrow Pt(111) - H \qquad (1)$$

On the other hand, positive charges can be related to the oxidative adsorption of anionic species

$$Pt(111) + A^{n-} \rightarrow Pt(111) - A^{m-} + (n - m)e \qquad (2)$$

where the adsorbed species A^{m-} can be formed either from the free species in solution, A^{n-}, or from another species linked to A^{n-} through a fast chemical equilibrium (see below). The transition between these two adsorption processes takes place in a potential region where the total charge density is zero at a characteristic electrode potential value. This is the so-called potential of zero total charge, pztc.[40,41] From the knowledge of the pztc value, an estimate of the potential of zero free charge (pzfc) is possible under some reasonable assumptions.[40,41]

The pztc value in the CO_2-containing solution is 0.33 V, that is, the same value observed in pure 0.1 M $HClO_4$ solution.[39] This behavior indicates that there is a negligible overlapping between hydrogen desorption and anion adsorption processes at the pztc. In perchloric acid solution, hydroxyl anions are suggested to be the anionic adsorbed species. As stated previously,[12,13] adsorbed anions in the CO_2-containing solution arise from the surface acid−base equilibrium of carbon dioxide that can give rise to the formation of either adsorbed bicarbonate

$$Pt(111) + CO_2 + H_2O \rightarrow Pt(111) - HCO_3^{x-} + H^+ + (1 - x)e \qquad (3)$$

or adsorbed carbonate anions[13]

$$Pt(111) + CO_2 + H_2O \rightarrow Pt(111) - CO_3^{y-} + 2H^+ + (2 - y)e \qquad (4)$$

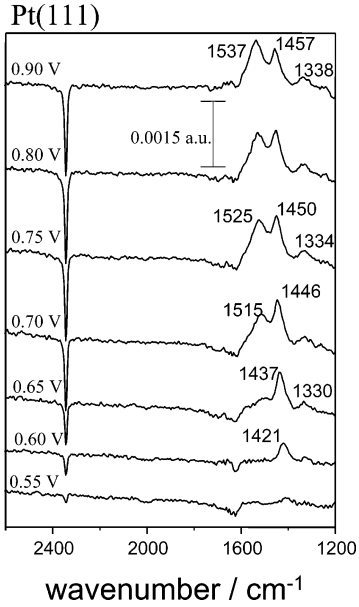

Figure 2. In-situ infrared spectra obtained at different potentials for a Pt(111) electrode in contact with a CO_2-saturated 0.1 M $HClO_4$ solution. Reference potential: 0.10 V. 500 interferograms were co-added at each electrode potential with p-polarized light.

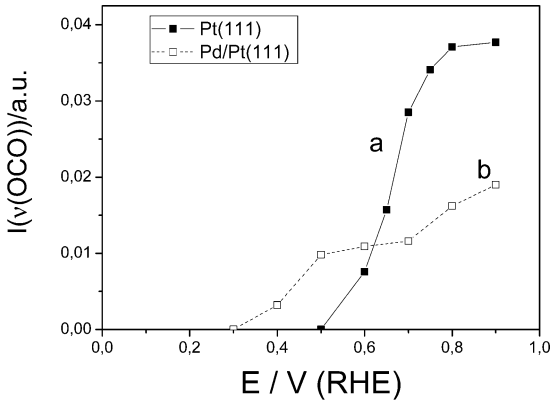

Figure 3. Plots of the integrated intensity of the CO_2 consumption bands observed in the spectra collected at different potentials for (a) Pt(111) (■) and (b) Pd/Pt(111) (□) electrodes in contact with a CO_2-saturated 0.1 M $HClO_4$ solution.

The occurrence of these surface reactions is witnessed by the in-situ infrared spectra reported in Figure 2 showing that carbon dioxide is consumed at potentials above 0.55 V. This consumption is reflected by the negative-going band at 2344 cm^{-1} corresponding to the asymmetric O−C−O stretching of dissolved carbon dioxide. The integrated intensity of this CO_2 band is plotted in Figure 3, curve a, as a function of the electrode potential. From the comparison of this plot with the voltammetric and the charge density curves in Figure 1B, it can be stated that the consumption of CO_2 is associated to the positive charge density values for potentials higher than 0.55 V. In addition, Figure 2 shows that the consumption of CO_2 is paralleled by the appearance of two main positive-going bands. One of these bands appears at 1421−1457 cm^{-1} for potentials above 0.55 V, whereas the second band is observed, for potentials higher than 0.65 V only, in the spectral region between 1515 and 1537 cm^{-1}. A third and less intense, positive-going band is observed at ca. 1330 cm^{-1} in connection with the band at 1421−1457 cm^{-1}. Figure 4 shows the potential dependent behavior of the frequency of these three bands that can be related to the formation of adsorbed species. This assignment is

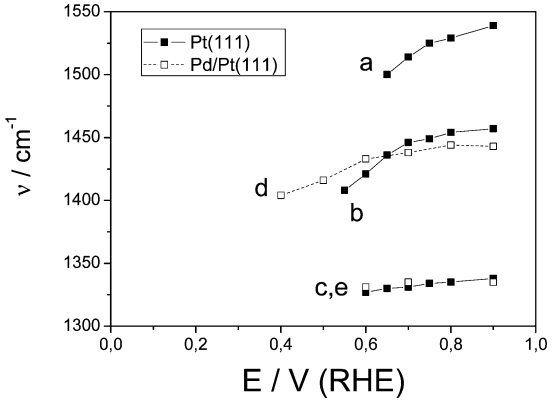

Figure 4. Plots of the frequency of the adsorbate bands observed in the spectra collected at different potentials for (a−c) Pt(111) (■) and (d,e) Pd/Pt(111) (□) electrodes in contact with a CO_2-saturated 0.1 M $HClO_4$ solution.

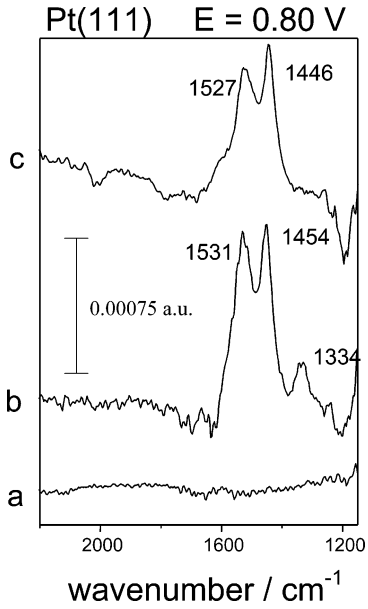

Figure 5. In-situ infrared spectra obtained at 0.80 V for a Pt(111) electrode in contact with CO_2-saturated 0.1 M $HClO_4$ solution prepared in water (a,b) or in deuterium oxide. (c) Spectrum a was collected with s-polarized light whereas spectra b and c were collected with p-polarized light. Reference potential: 0.10 V. The number of interferograms coadded at each electrode potential was 2000, 500, and 3000 for spectra a, b, and c, respectively.

confirmed by the absence of these bands in the spectra collected with s-polarized light (see spectrum a in Figure 5).

The observation of several adsorbate bands suggests either the coexistence of two different adsorbate species or of two different bonding modes of the same adsorbed species. The positive shift of the adsorbate bands when increasing the electrode potential is usually related to the effect of the electrode potential on the band frequency (Stark effect) as well as to the increase of dipole coupling associated to changes in the relative surface coverage of the corresponding species.[6] The increase in the total surface coverage of the adsorbed species is reflected by the increasing intensity of the CO_2 consumption band up to 0.90 V (see Figure 3, curve a). Comparing the FTIR spectra obtained in electrochemical environment to those corresponding to carbonato complexes, Iwasita et al.[13] assigned these bands to bidentate (bridge) and monodentate (on top) carbonate species. However, density functional theory based cluster model calculations[20] suggest an alternative assignment of the same bands to short- and long-bridge bonded carbonate anions.

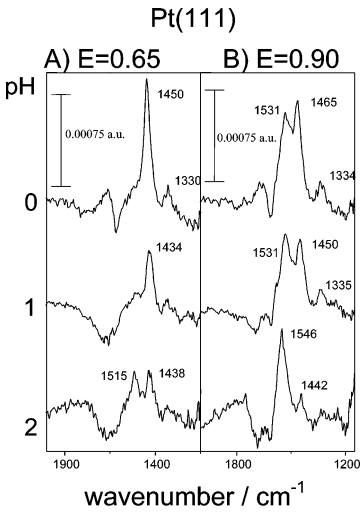

Figure 6. In-situ infrared spectra obtained at 0.65 and 0.90 V for a Pt(111) electrode in contact with CO_2-saturated 1.0 M $HClO_4$ (pH = 0), 0.1 M $HClO_4$ (pH = 1), and 0.01 M $HClO_4$ + 0.09 $KClO_4$ (pH = 2) solutions. Approximate pH values have been calculated as $-\log[H_3O^+]$. Reference potential: 0.10 V. 1000 interferograms were coadded at each electrode potential with p-polarized light.

Clearly, univocal assignments require further experimental and theoretical studies. These are described in detail in the next sections.

Series of potential-dependent spectra as those reported in Figure 2 were collected under the same experimental conditions but with a working solution prepared with deuterium oxide as a solvent. The aim of this kind of experiment was to check the existence of any isotopic effect on the frequency of the adsorbate bands observed for the Pt(111) electrode in the CO_2 saturated solution. The spectrum collected at 0.80 V under these conditions (spectrum c) can be compared in Figure 5 with that collected at the same potential in water (spectrum b).

The main adsorbate bands appear at roughly the same frequency and with the same intensity in both spectra. However, the small feature appearing at 1330 cm^{-1} in the spectrum collected in water is not observed in the D_2O solution. This behavior strongly suggests that the corresponding vibration involves a hydrogen atom which is replaced by deuterium in the D_2O solution. On the other hand, experiments described above using 0.1 M $HClO_4$ (with a pH value roughly estimated as $-\log[H_3O^+] = 1$, i.e., considering activity equal to concentration) as test electrolyte have been extended to solutions with different pH values. Figure 6A and B shows spectra obtained at two different electrode potentials for the Pt(111) electrode in contact with CO_2-saturated 1.0 M $HClO_4$ (approximate pH around 0) and 0.01 M $HClO_4$ + 0.09 M $KClO_4$ (approximate pH around 2), respectively.

These spectra can be compared in the same figure with those collected at the same electrode potential in a 0.1 M $HClO_4$ solution. The main effect of pH on the infrared spectra is related to the relative intensity of the adsorbate bands. Namely, increasing the solution pH gives rise to an increase of the relative intensity of the adsorbate band above 1500 cm^{-1} with respect to the band observed at lower frequencies. In this way, this band predominates in the spectra collected at 0.90 V in the less acidic solution. Experiments performed in solutions with pH higher than 2 gave spectra where the total intensity of the adsorbate band decreased. This latter behavior, that can be related to the competitive adsorption of hydroxyl species, was paralleled by a lower intensity of the carbon dioxide consumption band as well as by a smaller effect of the presence of carbon dioxide

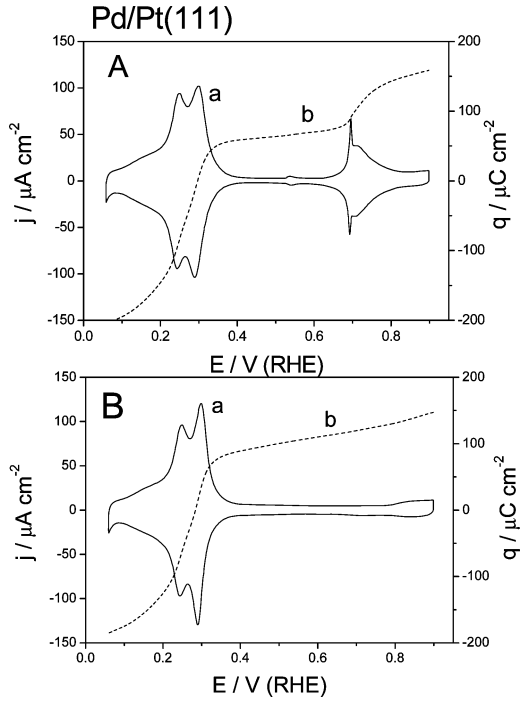

Figure 7. Cyclic voltammograms (a) and charge density curves (b) obtained for a Pd/Pt(111) electrode in (A) a CO_2-free and (B) a CO_2-saturated 0.1 M $HClO_4$ solution.

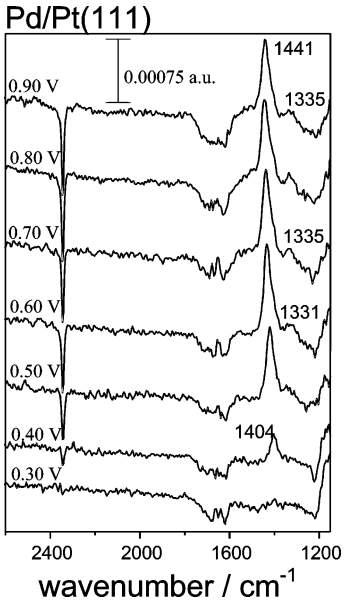

Figure 8. In-situ infrared spectra obtained at different potentials for a Pd/Pt(111) electrode in contact with a CO_2-saturated 0.1 M $HClO_4$ solution. Reference potential: 0.10 V. 500 interferograms were coadded at each electrode potential with p-polarized light. Wavenumbers are in cm^{-1}.

on the voltammetric features characteristic of the Pt(111) electrode in the working solution. The negative-going bands observed in Figure 6 between 1600 and 1800 cm^{-1}, also observed in the spectra reported in Figure 2, are related to the infrared absorption from water molecules which is uncompensated when stepping the electrode potential from the reference to the sample potential because of the thin-layer configuration.[6] Obviously, these features do not appear in the spectra collected in the D_2O solution.

2c. Experimental Results for Pd/Pt(111) Electrodes. Curve a in Figure 7A shows the cyclic voltammogram obtained, in the perchloric acid solution free of carbon dioxide, for a palladium monolayer deposited on a Pt(111) electrode. This voltammogram is similar to those previously published.[30,42] Adsorption states appearing at potentials higher than 0.60 V, including the sharp spikes at 0.70 V, are characteristic of a well-ordered palladium monolayer and can be ascribed to the adsorption/desorption of oxygenated (hydroxyl) species. CO displacement experiments performed for the palladium-covered Pt(111) electrode in the absence of carbon dioxide allowed the calculation of the corresponding total charge density curve (curve b in Figure 7A). Negative charge densities at potentials close to the hydrogen evolution are higher than in the palladium-free electrode (Figure 1A), thus indicating the achievement of a higher hydrogen coverage (closer to the full monolayer).[30,42] On the other hand, the observation of positive total charge densities at potentials higher than 0.30 V (curve b in Figure 7A) reflects that the measured pztc (around 0.30 V) is the result of contributions of the free charge that compensate hydrogen adsorption.[30] A lower pzfc for the palladium-covered electrode may be expected from the lower value of the work function of palladium when compared to that of platinum.[30]

Curves a and b in Figure 7B were obtained for the palladium monolayer in the CO_2-saturated solution. The cyclic voltammogram obtained under these conditions (curve a) is similar to that obtained in the absence of CO_2 except for the absence of the adsorption states between 0.60 and 0.80 V. The pztc value, around 0.29 V, is somewhat lower than that observed in the absence of carbon dioxide. This behavior would suggest that adsorption from carbon dioxide takes place at potentials lower than on the bare Pt(111) electrode surface. Despite the absence of the voltammetric features above 0.70 V when carbon dioxide is present in the working solution, the total charge density value attained at potentials around 0.90 V is roughly the same as that reached in the CO_2-free solution. This behavior, which can be connected with the observation of higher current densities in the potential region between 0.40 and 0.60 V, suggests the existence, in this potential region, of adsorption processes in addition to pure capacity (double-layer) charging.

The in-situ infrared spectra obtained for the Pd/Pt(111) electrode in the presence of carbon dioxide are reported in Figure 8. Adsorbate bands appear at potentials higher than 0.40 V (i.e., at potential ca. 0.2 V lower than for the palladium-free electrode) in parallel to a consumption band for carbon dioxide. A plot of the integrated intensity of this latter band as a function of the electrode potential is shown in Figure 3, curve b, where it can be compared to the data discussed above for the Pt(111) electrode. The intensity of the CO_2 band in the potential region around 0.90 V is significantly lower for the palladium-covered electrode, thus suggesting the achievement of a lower adsorbate coverage. Regarding the adsorbate features, a positive-going band is observed for the palladium monolayer with its maximum ranging from 1404 to 1441 cm^{-1}. This band is paralleled by a less intense band at ca. 1330 cm^{-1}. As a difference with the spectra reported in Figure 2 for the Pt(111) electrode, no significant positive band is observed above 1500 cm^{-1} in the spectra shown in Figure 8. Plots for the band frequency of the observed adsorbate bands are given in Figure 4, curves d and e.

As in the Pt(111) electrode, additional experiments were performed to check the effect of the eventual deuteration of the adsorbed species and the effect of solution pH on the spectra obtained for the palladium monolayer. In this way, it has been

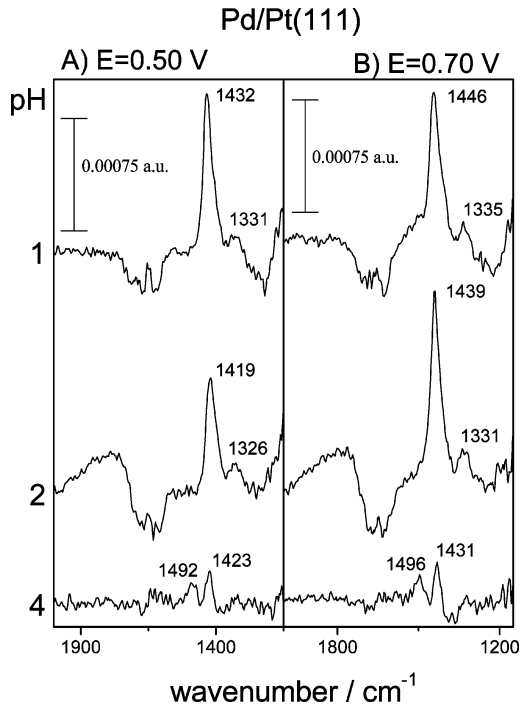

Figure 9. In-situ infrared spectra obtained at 0.50 and 0.70 V for a Pd/Pt(111) electrode in contact with CO_2-saturated 0.1 M $HClO_4$ (pH = 1), 0.01 M $HClO_4$ + 0.09 $KClO_4$ (pH = 2), and 0.1 mM $HClO_4$ + 0.1 M $KClO_4$ (pH = 4) solutions. Approximate pH values have been calculated as $-\log[H_3O^+]$. Reference potential: 0.10 V. 1000 interferograms were coadded at each electrode potential with p-polarized light.

verified that the band between 1400 and 1441 cm^{-1} is also observed in the spectra collected in a D_2O solution whereas that around 1330 cm^{-1} disappears. The effect of changing the solution pH can be appreciated in the spectra reported in Figure 9. No adsorbate band is observed above 1500 cm^{-1} in the spectra collected at pH around 2. The same behavior is observed at pH around 3. The decreasing frequency of the adsorbate band observed around 1430 cm^{-1} for a given electrode potential when increasing the solution pH can be related to the existence of lower adsorbate coverage because of the competitive adsorption of hydroxylated species. The spectra reported for a solution with a pH around 4 show that the intensity of the adsorbate band has greatly decreased under these conditions. However, a small feature is observed around 1490 cm^{-1} together with the small adsorbate band at 1423 cm^{-1} that could be related to the adsorbate band observed above 1500 cm^{-1} for the Pt(111) electrode.

3. Theoretical Section

3a. Computational Details. The interaction of carbonate with platinum, palladium, and bimetallic platinum−palladium surfaces has been studied using DFT methods and slab models. The calculations were performed with the Vienna Ab initio Simulation Package (VASP).[43,44] In this code, a plane wave basis set is used to expand density and exploits the advantages of the projector augmented-wave (PAW) method to describe the effect of the core electrons on the valence density of the atoms.[45] The exchange-correlation functional used was the generalized gradient approximation (GGA) of Perdew and Wang (PW91);[46] a non-spin-polarized formalism was employed. The cutoff kinetic energy for the plane wave basis set was 400 eV. Smearing methods were used to speed-up the convergence in the SCF process; however, the final energy was always extrapolated to a situation when the smearing width is set to zero. The sampling over the Brillouin zone was performed on a 7 × 7 × 1 Monkhorts-Pack mesh of k-points.[47]

The metallic surfaces were modeled using the infinite repeated slab model where a section of the material of finite thickness and infinite two-dimensional periodicity is repeated in the direction perpendicular to the surface with a sufficiently large vacuum width between the repeated slabs. The slabs used contain four atomic layers, with the equivalent of six missed layers (∼15.8 Å) as a vacuum space between two slab images in the *z* axis. For the platinum and palladium systems, the initial positions of the metallic atoms in the slab were the bulk experimental ones, with a nearest-neighbor distance of 2.775 and 2.751 Å, respectively. Pd/Pt(111) surfaces consisting of a palladium monolayer deposited over platinum were also modeled in a similar way, placing a layer of palladium atoms on a three-layer platinum slab. For each system, the two uppermost layers of the metallic surface and the adsorbate were allowed to relax in all directions. The adsorbate was placed on one side of the slab. The fundamental lattice considered was the $(\sqrt{3}\times\sqrt{3})$-R30°, leading to a coverage of 0.33 monolayer (ML). In the Pt(111) electrode, this choice is based on the coverage estimation[13] for the adsorbed species formed from CO_2. This estimation was done by the comparing of the integrated intensity of the CO_2 consumption band observed in experiments as those reported in Figure 2 with the integrated intensity of the CO_2 band observed after the oxidative stripping of a CO monolayer adsorbed on a Pt(111) electrode.[13] Several starting structures for the adsorption modes were considered: three perpendicular ones, bidentate short bridge (sh-BD) and long bridge (lg-BD), monodentate O-top (O-t), and a flat orientation parallel to the surface (par). (see Figure 10).

In the short-bridge site, the adsorbate is sited with its symmetry plane perpendicular to the surface and two of the oxygen atoms pointing toward first-neighbor Pt top sites forming a short-bridge site in the surface. The long-bridge structure is similar to the short-bridge one, but now the top surface atoms interacting with the oxygen atoms are forming a long-bridge surface site. In the parallel structure, the carbonate is placed with the symmetry plane horizontal to the surface, with the carbon atom lying above a threefold fcc site and the oxygen atoms pointing toward three top sites. Finally, the O-top case was built in a monocoordinated way, with an oxygen atom placed on top a metal surface atom, and the two remaining oxygen atoms pointing outside the surface. The geometry of the adsorbate over the surface was fully optimized with the conjugate-gradient algorithm, without any imposed restrictions. Frequency calculations were performed numerically, constructing the Hessian matrix from small displacements of the adsorbate atoms, keeping the metallic atoms of the surface frozen. All the systems were taken as electrically neutral, since the two negative charges of the carbonate anion cannot be included in the periodical approach. Nevertheless, previous work[20] has shown that the final adsorbed species is always the same independently of whether the neutral molecule or the anion is initially placed on the surface model. Therefore, it is assumed that charge transfer from the metal to the adsorbate will occur naturally to reach the most favorable form for the adsorbate. In the view of the experimental results reported in the previous sections, the complete set of calculations described above was also repeated for bicarbonate.

To further investigate the effect of considering anionic species from the very beginning, test calculations were performed placing carbonate anions on top of a cluster model representation

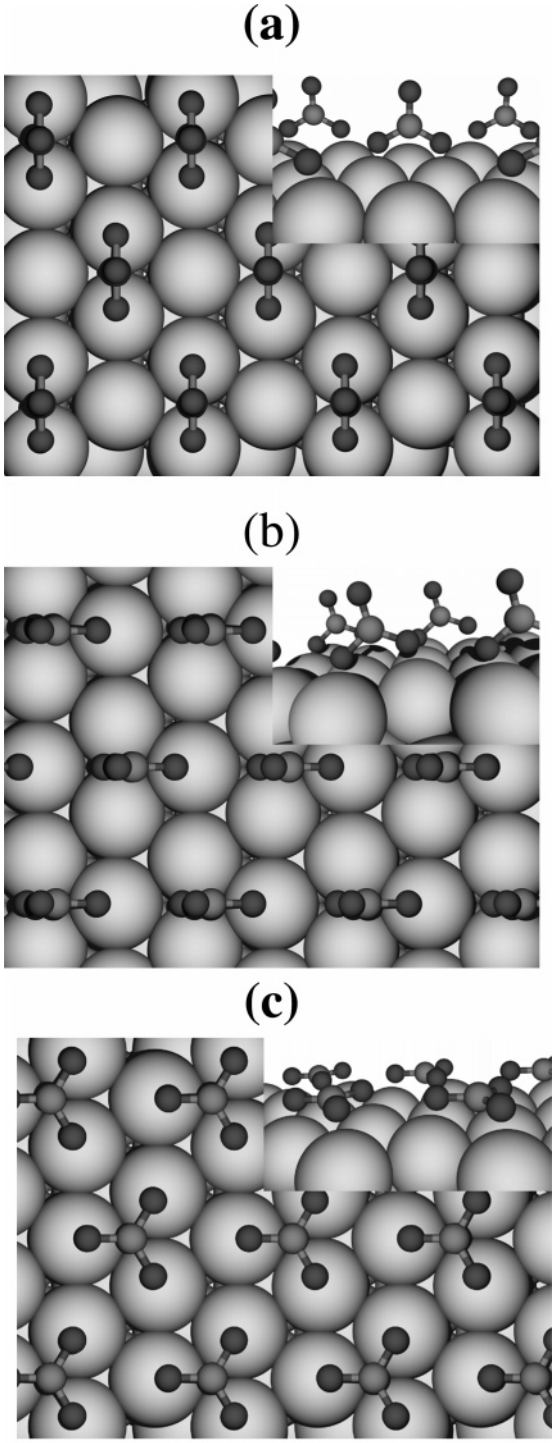

Figure 10. Schematic top and side views of carbonate adsorbed on the short-bridge (a) and long-bridge (b) sites and in the parallel mode (c). Shown is the $(\sqrt{3}x\sqrt{3}) - R30°$ periodicity of the lattice for the 0.33 coverage.

of the surface and using the hybrid B3LYP functional as implemented in the Gaussian 98 package.[48] A Pd_{22} cluster model containing 14 atoms in the first layer and 8 atoms in the second layer was used to represent Pd(111), see Figure 11. This cluster model ensures that all surface sites involved in the adsorption process are surrounded by the first and the second shell of neighbor atoms. It has been shown that this is a critical point when an accurate energetic description is desired.[49,50] In the cluster calculations, the $5s^2 5p^6 5d^{10}$ electrons of palladium were explicitly considered within the LANL2DZ basis set whereas the inner-core electrons were described by means of a relativistic

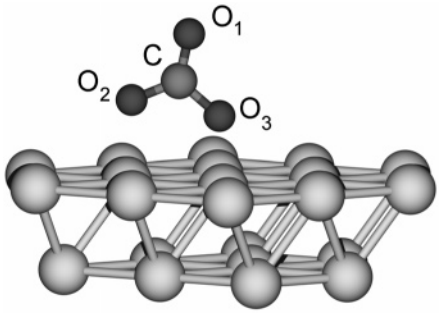

Figure 11. Schematic view of the 22 atom cluster model used in this study to model the (111) surface. Carbonate is adsorbed on the long-bridge site.

TABLE 1: Structural Data (Å and Degrees) and Binding Energy (eV) of Carbonate Adsorbed on Pd(111)[a]

	sh-BD	lg-BD	par	O-t
d_{C-O_1}	1.233	1.221	1.303	
d_{C-O_2}	1.317	1.303	1.303	
d_{C-O_3}	1.317	1.367	1.303	
$d_{O_2\text{-surf}}$	2.006	2.028	2.058	$CO_2 + O_{hcp}$
$d_{O_3\text{-surf}}$	2.006	1.671	2.059	
O_2CO_3	122.3	117.2	120.0	
BE	2.78	2.74	2.35	

[a] O_1 stands for the oxygen atom pointing outward the surface for sh-BD and lg-BD configurations. O_2 interacts on top a surface atom and O_3 over a bridge site on the surface for the lg-BD case. O_2 and O_3 are strictly equivalent in the sh-BD configuration, and all oxygen atoms are equivalent in the parallel configuration.

small-core pseudopotential. The basis set and pseudopotentials have been taken from Hay and Wadt.[51] For C and O, all electrons were explicitly considered within the standard 6-31G* basis set. Geometry optimizations were performed by means of the Berny algorithm using internal coordinates.

3b. Bonding Modes and Interaction Energies. The slab model geometry optimization of carbonate on the short-bridge site on the Pd leads to a structure which is very close to the initial guess; the adsorbate remains over the short-bridge site, with the oxygen atoms labeled O_2 and O_3 interacting in a bidentate fashion with two Pd atoms of the surface, as shown in Figure 10a. The distances from the carbon atom to the O_1 and to the two surface-bonded oxygen atoms (O_2 and O_3) differ by ~0.1 Å with a O_2-C-O_3 angle of 122.3° (see Table 1), and the initial D_{3h} symmetry group of the molecule has been reduced to C_{2v}. The long-bridge mode initial structure is similar to that of the short-bridge mode but in this case the oxygen atoms closer to the surface are pointing directly to palladium atoms forming a long bridge in the surface. However, the geometry optimization leads to a final arrangement where one of the oxygen atoms (O_2) interacts directly with a palladium surface atom (on top interaction), while the other oxygen (O_3) is pointing toward a bridge site between two palladium atoms and the adsorbate is slightly tilted (see Figure 10b). For the flat adsorption mode, the adsorbate is initially placed with its molecular plane parallel to the surface. In the final optimized structure, the carbon atom is on an fcc hollow site, with the three oxygen atoms pointing toward the palladium atoms forming the hollow site (Figure 10c). The three C−O distances are almost equivalent, but the carbon atom lies out of the molecular plane. A similar structure has recently been found as the most stable one for CO_3 on Ag(110).[52] Finally, for the O-top configuration, where an oxygen atom interacts directly with a metal atom on the surface, the two uncoordinated oxygen atoms lie in almost above bridge sites and point outward to the

TABLE 2: Structural Data (Å and Degrees) and Binding Energy (eV) of Carbonate Adsorbed on Pt(111)

	sh-BD	lg-BD	par	O-t
d_{C-O_1}	1.229	1.215	1.306	
d_{C-O_2}	1.327	1.305	1.306	
d_{C-O_3}	1.327	1.393	1.306	
$d_{O_2\text{-surf}}$	2.025	2.057	2.085	par
$d_{O_3\text{-surf}}$	2.025	1.715	2.083	
O_2CO_3	122.9	116.9	120.0	
BE	2.79	2.68	2.33	

surface. However, upon geometry optimization this starting structure dissociates; an oxygen atom remains on the surface adsorbed in an hcp site and a CO_2 molecule desorbs from the surface. All final optimized structures exhibit a common trend; the distances between the carbon atom and the oxygen atoms directly interacting with the surface increase with respect to the values in the free CO_3 reference ($d_{C-O} = 1.264$ Å) calculated with the same methodology. On the other hand, the distances between the carbon atom and the oxygen atoms pointing out to the surface decrease. This is consistent with bond order conservation arguments as already suggested by Patrito et al.[53] in their study of carbonate species on Ag(111) and was also observed in the earlier theoretical study of carbonate on Pt-(111).[20] The fact that three equivalent C−O bonds are found in the flat adsorption mode also supports this statement.

Additional calculations for carbonate adsorbed on Pd(111) were also performed using cluster model calculations for the short- and long-bridge adsorption modes. In this case, the whole system carries a −2 net charge in an attempt to better model the adsorption of carbonate anion instead of that of carbon trioxide. Nevertheless, the final results agree quite well with the ones predicted from the uncharged periodic model indicating that the slab model permits the effective charge redistribution. For the sh-BD configuration, the distance between the carbon atom and the oxygen atom not coordinated with the surface (O_1) is 1.238 Å, comparable with 1.233 Å as shown in Table 1. The C−O_2 and the O_2-surface distances predicted by the two surface models are very similar and the same holds for the O_2CO_3 angle, 121.7° in the cluster calculation and 122.3° in the periodic model. The description of the structure of the adsorbate predicted by both models is therefore nearly the same. This is because the metal surface provides a sufficiently large source of electrons and can delocalize the extra charge in the bulk so that the final state will be identical whether an initially charged or uncharged adsorbate is chemisorbed.[54] This is also the case in the cluster calculations provided the model is large enough. Therefore, the initial charge of the adsorbate is not important, leading to the final same adsorbed species; this has been confirmed in subsequent works.[20,55] Hence, the use of a neutral or charged system has no effect on parameters referring to the adsorbed state, such as geometry or vibrational frequencies. Consequently, only results from the periodic approach will be used in the forthcoming discussion and the term carbonate (or bicarbonate) will be used to refer to the adsorbed species.

Results corresponding to the adsorption of carbonate on a Pt(111) surface (Table 2) are very similar to those discussed for Pd(111) and also compare with previous studies. The structures considered are the same as for the palladium surface, and similar optimized geometries were obtained although, in this case, the O-top mode leads to the parallel mode after optimization. Quite interestingly, the values in the present work for adsorption on the short-bridge adsorption site agree quite well with those obtained with a B3LYP functional and a Pt_{20} cluster.[20] A different situation is encountered when interaction

TABLE 3: Structural Data (Å and Degrees) and Binding Energy (eV) of Carbonate Adsorbed on Pd/Pt(111)

	sh-BD	lg-BD	par	O-t
d_{C-O_1}	1.234	1.220	1.303	
d_{C-O_2}	1.317	1.302	1.303	
d_{C-O_3}	1.317	1.375	1.303	
$d_{O_2\text{-surf}}$	2.006	2.030	2.053	$CO_2 + O_{hcp}$
$d_{O_3\text{-surf}}$	2.006	1.642	2.053	
O_2CO_3	122.2	117.2	120.0	
BE	2.86	2.88	2.52	

TABLE 4: Structural Data (Å and Degrees) and Binding Energy (eV) of Bicarbonate Adsorbed on Pd(111)

	sh-BD	lg-BD	par	O-t
d_{H-O_1}	0.979	0.982		
d_{C-O_1}	1.359	1.351		
d_{C-O_2}	1.265	1.254		
d_{C-O_3}	1.275	1.291	sh-BD	$CO_2 + OH_{ads}$
$d_{O_2\text{-surf}}$	2.127	2.260		
$d_{O_3\text{-surf}}$	2.096	1.758		
O_2CO_3	129.2	126.4		
BE	2.53	2.25		

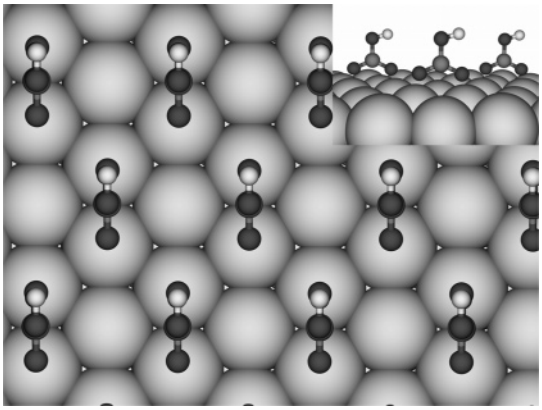

Figure 12. Schematic top and side views of bicarbonate adsorbed on the short-bridge site.

on the long bridge is considered. However, this is essentially due to the use of symmetry restrictions in the previous work.

The interaction of carbonate on a palladium monolayer on Pt(111) was simulated with a model consisting of a single layer of palladium atoms placed above a slab of three layers of platinum atoms. In this case, the two uppermost slab layers were also allowed to relax in the optimization process. Results for the different structures studied are summarized in Table 3. For the different adsorption modes, the geometrical parameters are almost the same as the case for palladium surfaces. Similarly, for the O-top adsorption case, carbonate dissociates into a molecule of CO_2 and an oxygen atom adsorbed on an hcp surface site. Moreover, the short- and long-bridge adsorption energies are very similar as for the clean Pd(111) surface. These results indicate that the second layer has only little influence in the resulting chemistry.

Finally, we consider the possibility that the adsorbed species is bicarbonate. Results for the bicarbonate model adsorbed on Pd(111) are shown in Table 4. Compared to carbonate, in the short-bridge case (Figure 12) the distance C−O_1 (1.359 Å) has been elongated, a direct effect of the hydrogen atom directly bonded to the O_1 atom; at the same time, the C−O_2 and C−O_3 distances decrease. Consequently, the most significant differential effect in the structure of adsorbed carbonate and bicarbonate is that in the latter the distances C−O_2 and C−O_3 are smaller than C−O_1 whereas the contrary holds for carbonate adsorption on the same Pd(111) surface. For the long-bridge

TABLE 5: Structural Data (Å and Degrees) and Binding Energy (eV) of Bicarbonate Adsorbed on Pt(111)

	sh-BD	lg-BD	par	O-t
d_{H-O_1}	0.980	0.980		
d_{C-O_1}	1.358	1.358		
d_{C-O_2}	1.267	1.265		
d_{C-O_3}	1.277	1.272	sh-BD	$CO_2 + OH_{ads}$
$d_{O_2\text{-surf}}$	2.145	2.170		
$d_{O_3\text{-surf}}$	2.120	2.007		
O_2CO_3	130.1	127.6		
BE	2.45	2.10		

TABLE 6: Structural Data and Binding Energy of Bicarbonate Adsorbed on Pd/Pt(111)

	sh-BD	lg-BD	par	O-t
d_{H-O_1}	0.979	0.981		
d_{C-O_1}	1.359	1.351		
d_{C-O_2}	1.266	1.255		
d_{C-O_3}	1.276	1.290	sh-BD	$CO_2 + OH_{ads}$
$d_{O_2\text{-surf}}$	2.115	2.216		
$d_{O_3\text{-surf}}$	2.092	1.769		
O_2CO_3	129.3	126.7		
BE	2.65	2.42		

mode, the same trend is observed, although the $C-O_1$ and $C-O_3$ distances are nearer. The molecule is now strongly tilted, since the distance from the oxygen positioned on top a surface palladium atom is largely increased with regard to adsorbed carbonate. Also, the O_2CO_3 angle has been increased for both adsorption modes in comparison with the values in Table 1. The optimization starting from the flat geometry leads to the same structure obtained for the short-bridge adsorption site and the O-top system is also not stable for bicarbonate, leading to the dissociation of the adsorbate. A OH molecule remains interacting with the surface, while a molecule of CO_2 moves away from the system. For all the stable sites, short and long bridge, the binding energies of bicarbonate are significantly smaller than those of carbonate ones on the Pd(111) surface. Analogous results are obtained for the Pt(111) and Pd/Pt(111) systems, summarized in Tables 5 and 6.

The values of the interaction energies deserve a further comment. The reported values are obtained with respect to the separated uncharged systems. This has no effect on the relative energy of the same species on different sites but it makes very difficult an accurate comparison between the adsorption energies of carbonate and bicarbonate. Therefore, the following discussion will not make use of adsorption energy differences concerning different species and will focus on vibrational frequencies only.

4. Analysis of the Vibrational Frequencies and Discussion

On the basis of the calculated data discussed above regarding the stability of the adsorbed carbonate and bicarbonate, only the vibrational frequencies for the most stable adsorption sites, namely, short bridge and long bridge, will be considered in the following (Tables 7 and 8). Two points have to be taken into account when comparing the experimental spectra with the calculated data reported in these tables. First of all, the surface selection rule that makes that only the vibrational modes for adsorbed species giving rise to an oscillating dipole moment perpendicular to the metal surface are infrared active (see the discussion below). Second, the experimental conditions employed that avoid the observation of absorption bands lying below 1100 cm^{-1} because of both the interference of perchlorate anions in the test electrolyte and the cutoff in the transmission of the calcium fluoride window. In the same sense, bands appearing above 3000 cm^{-1} would be hardly observed because of the strong infrared absorption from water in this spectral region.

TABLE 7: Vibrational Frequencies (cm^{-1}) of Carbonate Adsorbed on Pd(111), Pt(111), and Pd/Pt(111) for the Most Stable Adsorption Sites, Short-Bridge and Long-Bridge[a]

	sh-BD				lg-BD		
MNV	Pd	Pt	Pd/Pt	MNV	Pd	Pt	Pd/Pt
$\nu(CO_1)$	1577	1591	1571	$\nu(CO_1)$	1643	1686	1648
$\nu_{as}(CO)$	1214	1177	1212	$\nu(CO_2)$	1158	1140	1159
$\nu_s(CO)$	971	937	973	$\nu(CO_3)$	875	822	856
$\pi(C)$	706	699	709	$\pi(C)$	734	734	737
δ (OCO)	626	639	628	δ(OCO)	652	674	652
δ (OCO)	617	631	613	δ(OCO)	579	584	583

[a] O_2 and O_3 are strictly equivalent in the sh-BD configuration; therefore, a local C_{2v} symmetry exists, leading to the appearance of a symmetric and antisymmetric stretching of carbon with the surface-coordinated oxygen atoms (ν_s and ν_{as}). These normal modes are not degenerated for the lg-BD case, since the local symmetry is broken. $\pi(C)$ stands for the out-of-plane mode of carbon atom and δ(OCO) is the deformation mode altering the angles between the atoms.

TABLE 8: Vibrational Frequencies (cm^{-1}) of Bicarbonate Adsorbed on Pd(111), Pt(111), and Pd/Pt(111) for the Most Stable Adsorption Sites, Short-Bridge and Long-Bridge[a]

	sh-BD				lg-BD		
MNV	Pd	Pt	Pd/Pt	MNV	Pd	Pt	Pd/Pt
$\nu(HO_1)$	3659	3660	3660	$\nu(HO_1)$	3618	3663	3633
$\nu_{as}(CO)$	1507	1528	1524	$\nu(CO_2)$	1536	1526	1536
$\nu(CO_1)$	1409	1412	1415	$\nu(CO_1)$	1402	1425	1408
$\delta(HO_1C)$	1212	1218	1213	$\delta(HO_1C)$	1206	1215	1212
$\nu_s(CO)$	1020	1022	1021	$\nu(CO_3)$	1022	1031	1025
$\pi(C)$	740	742	747	$\pi(C)$	755	754	757
δ(OCO)	664	674	667	δ(OCO)	658	678	668
δ(OCO)	612	626	624	δ(OCO)	594	586	602
π(H)	514	523	534	π(H)	582	556	592

[a] $\delta(HO_1C)$ stands for the in-plane bending of the hydrogen atom, and π(H) is the out-of-plane deformation of the hydrogen atom.

The most relevant vibrational modes for adsorbed carbonate (Table 7) are those related to the $A_{1'}$ mode of the free carbonate molecule. This is because the corresponding adsorption bands can be clearly identified in the explored region of the infrared spectrum. It has to be recalled here the absence of significant isotopic effects on the main adsorbate bands when replacing water by deuterium oxide in the experiments reported in Figure 5 (as well as in similar experiments performed for the palladium monolayer). This behavior suggests that these features are related to vibrational modes involving C−O bonds. Moreover, the calculation of the intensity of the normal modes (by means of a numerical estimate of the dipole moment derivatives, $d\mu_z/dz$) shows that only the $\nu(CO_1)$ mode is significantly intense. The origin of the small adsorbate band at ca. 1330 cm^{-1}, which is not observed in the D_2O solution, will be discussed later. For the same adsorption site, comparison of the values between the different surfaces reveals that the $C-O_1$ stretching frequencies are slightly higher on Pt(111) than on Pd(111), in agreement with the shorter $C-O_1$ distances for the Pt(111) case. Another interesting trend is the fact that these vibrational frequencies are only determined by the nature of the topmost atomic layer as previously found for CO on Pd/Pt(111), Pd(111), and Pt(111) surfaces.[31] The frequencies for the bicarbonate system has also been calculated and presented in Table 8. The main structural

effect of the extra hydrogen atom, the increasing of the $C-O_1$ distance, leads to a concomitant decrease in the vibrational frequency. In this case, the most intense normal mode is again the $\nu(CO_1)$ one, but the $\delta(HO_1C)$ mode has a relative intensity ~20% and should be detected in the spectrum.

From the present calculated values (Table 7), it appears that the corresponding vibrational frequency of carbonate adsorbed on a long-bridge site always appears at ~80 cm^{-1} above that corresponding to the short-bridge adsorption site. For the Pt(111) surface, a first comparison of the theoretical results with the experimental spectra shown in Figures 2, 5, and 6 suggests to assign the feature appearing at the highest potential at ~1457 cm^{-1} to the carbonate adsorbed in a short-bridge site and the feature appearing at ~1537 cm^{-1} to the long-bridge chemisorbed carbonate. The difference in the frequencies between the two features in the experimental spectrum is ~80 cm^{-1}, very close to the theoretical gap of ~95 cm^{-1}, providing additional support to this assignment. The present interpretation is consistent with that made by Markovits et al.[20] but with the reverse order. This difference can be attributed to the use of symmetry restrictions in the previous model calculations which results in quite a different structure for the long-bridge site. Nevertheless, the assignment above is puzzling because the absolute value of the theoretical frequencies is always ~130−150 cm^{-1} larger than the experimental values obtained at 0.9 V. In this respect, theoretical values do not take into account the external potential applied during the spectroelectrochemical experiments, and frequencies for a given adsorbate are affected by the surface potential. In the electrochemical interfaces, frequencies can be expected to be lower than those observed for the same adsorbate in the metal/vacuum interfaces because of the existence of a lower absolute surface potential in the electrochemical environment.[56] However, these effects do not seem to be enough to justify the reported difference between experimental and calculated frequencies for adsorbed carbonate. In fact, vibrational frequencies for urea adsorbed on Pt(100) electrodes predicted from cluster model calculations in absence of electric field effects are much closer to the experimental values.[57]

The absolute values of the calculated results suggest an alternative interpretation that involves the adsorption of bicarbonate anions. In that case, comparison between calculated and experimental values strongly suggests that the feature in the IR spectrum corresponding to the Pt(111) electrode and appearing at 1421 cm^{-1} at 0.6 V (Figure 2) could be also ascribed to bicarbonate adsorbed on a short-bridge site. The theoretical value for the frequency is 1412 cm^{-1} and indeed this is the most stable adsorption site. The second band in the spectra of Figure 2 shows up in the 1515−1537 cm^{-1} range but only at potentials higher than 0.65 V. Interestingly, this potential coincides with a clear feature in the voltammogram of Figure 1B (curve a). This feature strongly suggests that under these electrochemical conditions a new species is formed involving a charge-transfer process. This statement seems to indicate that the new species could be carbonate, formed either from carbon dioxide (as reflected in eq 4) or from adsorbed bicarbonate (eq 5).

$$Pt(111) - CO_3H^{x-} \rightarrow Pt(111) - CO_3^{y-} + H^+ + (1 + x - y)e \quad (5)$$

This surface acid−base reaction is also supported from the pH-dependent behavior reported in Figure 6 for the spectra obtained for the Pt(111) electrode in the CO_2-saturated solution. From these spectra, it can also be concluded that the dissociation of adsorbed bicarbonate, as an intermediate stage in the adsorption process from carbon dioxide, takes place at lower pH values than in solution. In other words, the dissociation constant for adsorbed bicarbonate is higher than in solution. This statement can be connected with the observation of either bicarbonate or carbonate adsorbed species in a solution where the prevailing species at the working solution pH is carbon dioxide, thus involving higher equilibrium constant for reactions 3 and 4 than those typically observed in solution. Similar behavior has been observed for other weak acids such as acetic[14] and oxalic[18] acids on platinum electrodes. However, this is not a general trend since lower values than that observed in solution have been found for the potential-dependent dissociation constant of bisulfate adsorbed at a Pt(111) electrode surface.[17] Regarding the adsorption site for adsorbed carbonate on Pt(111), it has to be noticed that long-bridge and short-bridge sites are almost energetically degenerate. However, the calculated frequencies are different enough to assign the band observed above 1500 cm^{-1} to short-bridge carbonate.

For the Pd/Pt(111) system, there is no feature in the voltamogramm at the potential region of 0.65 V, and this is consistent with the presence of only one main band, and therefore a single species, in the IR spectra. Following the same reasoning as for the platinum system, the band at 1404 cm^{-1} for potentials above 0.4 V in Figures 8 and 9 can be assigned to bicarbonate adsorbed to the short-bridge site for which the corresponding vibrational frequency is 1415 cm^{-1}. Contrarily to the Pt(111) surface, increasing the electrode potential does not lead to the evolution from bicarbonate to carbonate at the Pd/Pt(111) surface. This behavior has to be connected to the attainment of a lower surface coverage for the adsorbates formed from carbon dioxide when the Pt(111) electrode is covered by a palladium layer. This fact can be related to the coadsorption of hydroxyl anions which is favored at the palladium surface atoms. This coadsorption process is also suggested from the charge density curve since a similar charge is measured at 0.90 for Pt(111) and Pd/Pt(111) whereas the consumption of carbon dioxide is lower in the latter case. The surface sites occupied by adsorbed OH would not be available for the adsorption of carbonate species. Since the bands for adsorbed carbonate are not observed even at a solution pH around 2, for which the carbonate feature prevails in the case of the bare Pt(111) electrode, it can be stated that the dissociation constant for adsorbed bicarbonate at palladium-covered Pt(111) electrodes is lower than that on Pt(111).

The origin of the small adsorbate band at ca. 1330 cm^{-1} deserves some further comments. This is the only feature that is affected by the change of water by deuterium oxide as the solvent for the spectroelectrochemical experiments. This behavior, together with the observation of this feature in parallel to the band between 1400 and 1460 cm^{-1}, suggests assigning it to a vibrational mode of adsorbed bicarbonate thus reinforcing the theoretical interpretation of the spectrum given above. Indeed, this feature was also ascribed to adsorbed bicarbonate, but to the symmetric OCO stretch mode of bidentate bicarbonate, although coadsorption of water was invoked to explain the small effect of the electrode potential on the frequency of the observed band.[13] From the data reported in Table 8 and from the fact that the 1330 cm^{-1} band is not observed in the D_2O solution, it is justified to assign this band to the HO_1C bending mode of adsorbed bicarbonate. However, this assignment cannot be done without warnings, because the structure of adsorbed bicarbonate indicates that solvent may play a strong influence on this vibrational mode, which is not the case for CO related modes.[20,57]

5. Conclusions

In this work, a combined in-situ spectroelectrochemical and theoretical study of carbonate and bicarbonate anions adsorbed on Pt(111) and Pd/Pt(111) electrodes is presented. These species are formed in a potential-dependent adsorption−desorption process from a perchloric acid solution saturated with CO_2, thus proving the existence of surface acid−base constants which are different from those observed in solution. For the Pt(111) electrode, the combination of voltammetric and FTIR results suggest that adsorbed carbonate can be formed either from carbon dioxide or from adsorbed bicarbonate anions in a charge-transfer process that takes place at potentials above 0.65 V. The relative surface coverages of adsorbed carbonate and bicarbonate depend on both the electrode potential and the solution pH. This is not the case for the palladium-covered platinum electrode, in which a single species is apparently present in all the ranges of potentials studied. Although direct assignations of the bands in the vibrational spectra are not straightforward, density functional model calculations permits one to distinguish among two possible different interpretations. In one case, the bands appearing in the FTIR spectra for platinum and palladium-covered platinum electrodes would be attributed to carbonate molecules interacting on different adsorption sites in the metallic surface. However, the too large difference ($\sim$130−150 cm^{-1}) between the experimental and calculated values suggests that an alternative assignment is needed. Therefore, it is proposed that the initial features shown in both Pt(111) and Pd/Pt(111) spectra at lower potentials are due to bicarbonate molecules adsorbed in a short-bridge bidentate configuration. In this case, the difference between experimental and calculations on a model system is reduced to at most 30 cm^{-1}. This interpretation is consistent with various observations. First, at the platinum electrode, the formation of carbonate is followed by the appearance of a new band at higher frequencies. Second, for the palladium-covered platinum electrode, this reaction is not observed and only bicarbonate molecules in a short-bridge configuration are expected to be found in the metallic surface. Finally, the isotopic effects on the band appearing at ca. $\sim$1330 cm^{-1} provide direct evidence of the presence of adsorbed bicarbonate.

As a more general conclusion, the present study shows that the combined use of spectroelectrochemical experiments and first principles calculations is a powerful tool for the interpretation of complex electrochemical interfaces.

Acknowledgment. Financial support has been provided by Spanish BQU2002-04029-CO2 (01 and 02), BQU2004-04029, and Catalan 2001SGR00315, 2001SGR00043, and Distinció de la Generalitat de Catalunya per a la Promoció de la Recerca Universitària (F.I.) projects. Finantial support from the Conselleria de Cultura, Educació i Ciència de la Generalitat Valenciana (Grupos03/208) is also acknowledged. Part of the computer time was provided by the CESCA/CEPBA/CIRI supercomputer centers through generous grants from Universitat de Barcelona, Fundació Catalana per a la Recerca and CIRI. A.G. and A.B. are indebted, respectively, to the University Rovira i Virgili and to the Ministerio de Ciencia y Tecnología for their predoctoral grants.

References and Notes

(1) *Comprehensive Treatise of Electrochemistry, The Double Layer*; Bockris, J. O'M., Conway, B. E., Yeager, E., Eds.; Plenum Press: New York, 1980; Vol. 1.

(2) Bockris, J. O'M.; Khan, S. U. M. In *Surface Electrochemistry. A Molecular Approach*; Plenum Press: New York, 1993.

(3) *Interfacial Electrochemistry: Theory, Experiments and Applications*; Wieckowski, A., Ed.; Marcel Dekker Inc.: New York, 1999.

(4) Clavilier, J. *J. Electroanal. Chem.* **1980**, *107*, 211.

(5) Clavilier, J.; Armand, D.; Sun, S. G.; Petit, M. *J. Electroanal. Chem.* **1986**, *205*, 267.

(6) Iwasita, T.; Nart, F. C. (a) In *Advances in Electrochemical Science and Engineering*; Gerischer, H., Tobias, C. W., Eds.; VCH: Weinheim, Germany, 1995; Vol. 4, Chapter 3. (b) *Prog. Surf. Sci*. **1997**, *55*, 271.

(7) Korzeniewski, C. *Crit. Rev. Anal. Chem.* **1997**, *27*, 81.

(8) Rodes, A.; Pérez, J. M.; Aldaz, A. In *Handbook of Fuel Cells: Fundamentals, Technology and Applications*; Vielstich, W., Lamm, A., Gasteiger, H. A., Eds.; John Wiley: Chichester, U.K., 2003; p 191.

(9) Faguy, P. W.; Marinkovic, N. S. *Langmuir* **1996**, *12*, 243.

(10) Nart, F. C.; Iwasita, T.; Weber, M. *Electrochim. Acta* **1994**, *39*, 961.

(11) Rodes, A.; Pastor, E.; Iwasita, T. *J. Electroanal. Chem.* **1994**, *369*, 183.

(12) Rodes, A.; Pastor, E.; Iwasita, T. *J. Electroanal. Chem.* **1994**, *373*, 171.

(13) Iwasita, T.; Rodes, A.; Pastor, E. *J. Electroanal. Chem.* **1995**, *383*, 181.

(14) Rodes, A.; Pastor, E.; Iwasita, T. *J. Electroanal. Chem.* **1994**, *376*, 109.

(15) Shingaya, Y.; Ito, M. *J. Electroanal. Chem.* **1999**, *467*, 299.

(16) Arihara, K.; Kitamura, F.; Osaka, T.; Tokuda, K. *J. Electroanal. Chem.* **2001**, *510*, 128.

(17) Lachenwitzer, A.; Li, N.; Lipkowski, J. *J. Electroanal. Chem.* **2002**, *532*, 85.

(18) Berná, A.; Rodes, A.; Feliu, J. M. *J. Electroanal. Chem.* **2004**, *563*, 49.

(19) Nakamoto, K. In *Infrared and Raman Spectra of Inorganic and Coordination Compounds*; John Wiley & Sons: New York, 1986.

(20) Markovits, A.; García-Hernández, M.; Ricart, J. M.; Illas; F. *J. Phys. Chem. B* **1999**, *103*, 509.

(21) Llorca, M. J.; Feliu, J. M.; Aldaz, A.; Clavilier, J. *J. Electroanal. Chem.* **1993**, *351*, 299.

(22) Baldauf, M.; Kolb, D. M. *Electrochim. Acta* **1993**, *38*, 2145.

(23) Inukai, J.; Ito, M. *J. Electroanal. Chem.* **1993**, *358*, 307.

(24) Attard, G.; Price, R.; Al-Akl, A. *Electrochim. Acta* **1994**, *39*, 1525.

(25) Gómez, R.; Rodes, A.; Pérez, J. M.; Feliu, J. M.; Aldaz; A. *Surf. Sci.* **1995**, *327*, 202.

(26) Naohara, H.; Ye, S.; Uosaki, K. *J. Phys. Chem. B* **1998**, *102*, 4366.

(27) Álvarez, B.; Rodes, A.; Pérez, J. M.; Feliu, J. M.; Rodríguez, J. L.; Pastor, E. *Langmuir* **2000**, *16*, 4695.

(28) Markovic, N. M.; Lucas, C. A.; Climent, V.; Stamenkovic, V.; Ross, P. N. *Surf. Sci.* **2000**, *465*, 103.

(29) Álvarez, B.; Climent, V.; Rodes, A.; Feliu, J. M. *J. Electroanal. Chem.* **2001**, *497*, 125.

(30) Álvarez, B.; Climent, V.; Rodes, A.; Feliu, J. M. *Phys. Chem. Chem. Phys*. **2001**, *3*, 3269.

(31) Gil, A.; Clotet, A.; Ricart, J. M.; Illas, F.; Álvarez, B.; Rodes, A.; Feliu, J. M. *J. Phys. Chem. B* **2001**, *105*, 7263.

(32) Feliu, J. M.; Álvarez, B.; Climent, V.; Rodes, A. In *Thin Films: Preparation, Characterization, Applications;* Soriaga, M. P., Ed.; Kluwer Academic/Plenum Publishers: 2002; p 37.

(33) Arenz, M.; Stamenkovic, V.; Schmidt, T. J.; Wandelt, K.; Ross, P. N.; Markovic, N. M. *Surf. Sci.* **2002**, *506*, 287.

(34) Rodes, A.; Pastor, E.; Iwasita, T. *J. Electroanal. Chem.* **1994**, *377*, 215.

(35) Clavilier, J.; El Achi, K.; Petit, M.; Rodes, A.; Zamakhchari, M. A. *J. Electroanal. Chem.* **1990**, *295*, 333.

(36) Clavilier, J.; Albalat, R.; Gómez, R.; Orts, J. M.; Feliu, J. M. *J. Electroanal. Chem.* **1993**, *360*, 325.

(37) Orts, J. M.; Gómez, R.; Feliu, J. M.; Aldaz, A. *Electrochim. Acta* **1994**, *39*, 1519.

(38) Iwasita, T.; Nart, F. C.; Vielstich, W. *Ber. Bunsen-Ges. Phys. Chem.* **1990**, *94*, 1030.

(39) Climent, V.; Gómez, R.; Orts, J. M.; Rodes, A.; Aldaz, A.; Feliu, J. M. In *Interfacial Electrochemistry: Theory, Experiments and Applications*; Wieckowski, A., Ed.; Marcel Dekker: New York, 1999; Chapter 26.

(40) Weaver, M. J. *Langmuir* **1998**, *14*, 3932.

(41) Climent, V.; Gómez, R.; Orts, J. M.; Aldaz, A.; Feliu, J. M. In *Electrochemical Double Layer;* Korzeniewski, C., Conway, B. E., Eds.; The Electrochemical Society: 1997; Vol. 97−17, p 222.

(42) Álvarez, B.; Feliu, J. M.; Clavilier, J. *Electrochem. Com.* **2002**, *4*, 379.

(43) Kresse, G.; Hafner, J. *Phys. Rev. B* **1993**, *47*, RC558.

(44) Kresse, G.; Furthmüller, J. *Phys. Rev. B* **1996**, *54*, 11169.

(45) Kresse, G.; Joubert, D. *Phys. Rev. B* **1998**, *59*, 1758.

(46) Perdew, J. P.; Chevary, J. A.; Vosko, S. H.; Jackson, K. A.; Pederson, M. R.; Singh, D. J.; Fiolhais, C. *Phys. Rev. B* **1992**, *46*, 6671.

(47) Monkhorst, H. J.; Pack, J. D. *Phys. Rev. B* **1976**, *13*, 5188.

(48) Frisch, M. J. et al.; Gaussian 98, Revision A.6; Gaussian Inc.: Pittsburgh, PA, 1998.
(49) Curulla, D.; Clotet, A.; Ricart, J. M.; Illas, F. *J. Phys. Chem. B* **1999**, *103*, 5246.
(50) Gil, A.; Clotet, A.; Ricart, J. M.; Kresse, G.; García-Hernández, M.; Rosch, N.; Sautet, P. *Surf. Sci.* **2003**, *530*, 71.
(51) Hay, P. J.; Wadt, W. R. *J. Chem. Phys.* **1985**, *82*, 299.
(52) Robinson, J.; Woodruff, D. P. *Surf. Sci*. **2004**, *556*, 193.
(53) Patrito, E. M.; Paredes Olivera, P. *Electrochim. Acta* **1998**, *44*, 1237.
(54) Paredes Olivera, P.; Patrito, E. M. *Electrochim. Acta* **1998**, *44*, 1247.
(55) Wasileski, S. A.; Weaver, M. J. *J. Electroanal. Chem.* **2002**, *524*, 219.
(56) Weaver, M. J.; Zou, S. Z.; Tang, C. *J. Chem. Phys.* **1999**, *111*, 368.
(57) García-Hernández, M.; Birkenheuer, U.; Hu, A.; Illas, F.; Rösch, N. *Surf. Sci.* **2001**, *471*, 151.